

# USING THE TEVATRON ELECTRON LENS (TEL) AS A WIRE AND OTHER TEL STUDIES AT FNAL

P. Lebrun, T. Sen, V. Shiltsev, X.L. Zhang, FNAL, Batavia, IL 60510, USA  
F. Zimmermann, CERN, Geneva, Switzerland

## *Abstract*

During a visit to FNAL, on March 1, 2004, we performed a two-dimensional grid scan - with 1-mm step size - of the TEL transverse position in the vicinity of the proton and pbar beams, while three bunches of either beam were excited by the TEL on every turn.

The measured tune shifts of protons and pbars are compatible with expectation. The proton Schottky 'emittance' is strongly dependent on the TEL position, possibly due to a coherent interaction between protons and electrons. The relative position of protons, pbars and TEL can be determined in three different ways: from the TEL BPM readings, from the tune variation with TEL position, and from the loss-rate variation with the TEL position. The results are consistent at least within 1 or 2 mm, possibly better. Tunes and losses do not necessarily yield identical values for the beam position. Significant proton losses occurred when the TEL approached the proton beam. These losses decreased with the third power of the distance. They were the result of a longitudinal shaving, which might be related to a longitudinal interaction of TEL and proton beam and/or to the nonzero dispersion at the TEL.

## MOTIVATION

We attempted to simulate the dynamic effects of the wire beam-beam compensation using the TEL. To this end we varied the electron beam positions transversely with respect to the proton and pbar beams so as to detect the effects on the proton beams, such as changes in beam loss, tunes and emittance, etc. At the same time, the two-dimensional TEL scan provides information on the exact 2-dimensional position of the proton and pbar orbits at the TEL as well as on the effect of the TEL on the proton beam, when it is centered on the pbars for TEL beam-beam compensation.

## SEQUENCE OF EVENTS

22:00 We measured Schottky spectra for the last bunch in each train. Later the gate was switched to the bunches A5, A17, A29 and P6, P18, P30. These numbers correspond to proton-pbar pairs which arrive at the TEL simultaneously (for example, A5 and P30 arrive at the same time). The TEL power supply was changed in order to increase the available current by ~15%.

22:20 Without TEL excitation, the TEL horizontal position was varied in steps of 1 mm over the range +4/-7 mm. At some intermediate region around -2.5 mm some proton losses were observed, possibly correlated with losses in the abort gap. The vertical proton orbit did not

move. We backed up and repeated the scan, and, the second time, there were no losses.

22:45 The same scan without excitation was conducted in the vertical plane over the range -5 mm, +3 mm. There were no losses and, thus, the available TEL aperture appeared sufficiently large for both planes.

22:55 Pbar RF water heater trip. Lost proton rate went up (why?).

23:00 TEL was set up in 3-pulse per turn mode. The TEL was first turned on in the abort gap and the electron current was maximized to about 600 mA. The abort gap was cleaned by exciting the lens every 7<sup>th</sup> turn (to remove gap particles generated by the RF trip). Then it was set back to every-turn mode and the timing was moved to the first proton bunch, finally to the 6<sup>th</sup> proton bunch. We remarked that the pbar tunes shifted, on the 1.7 GHz Schottky monitor readout. We moved the orbit towards the protons. The LOSTP signal increased for bunches P4, P5 and P6, with 6 showing the highest losses. There was no significant change in the proton-tune position noted, but the proton signal strength increased strongly. Next we moved the TEL beam towards the pbars. The pbar tune moved again. We also recorded some H and V spectra from the old Schottky monitor. A strong modulation at the synchrotron frequency was apparent in both spectra, perhaps indicative of the large chromaticity.

23:30-01:00 We scanned the TEL position around the pbar beam on a 1mm x 1mm grid.

01:00 We flew the wires and found little change in emittances.

01:00-01:40 We scanned the TEL position around the proton beam on a 1mm x 1mm grid. We recorded the loss-rate signals BOPLOS[i], B0ALOS[i], LOSTP, LOSTPB, D0PHTL, D0AHTL, D0AHTL[i], D0PHTL[i], etc. There was a significant increase in the proton loss rate in the immediate vicinity of the proton beam.

01:41 We scanned the TEL angle by 10 kG mm at TEL Position +2.5 mm, +1.5 mm.

We flew the wires again at the end. There was a certain increase in proton emittance and a more pronounced decrease in bunch length. This suggests that the TEL caused a longitudinal shaving of the protons.

## RESULTS

### *TEL Set Up*

A few TEL parameters are compiled in Table 1 and the positions of the three beams upstream and downstream of the TEL in Table 2. We note that there is about 2 m dispersion at the TEL. The beam positions were measured before the start of the study with the TEL in nominal position and timed on the abort gap. The TEL position is

controlled by 6 correctors: T:L1C1, T:L1C2,... where L1C2 relates to the Y position, L1C4 to the X position. The correctors are excited in combinations of 2 or 4, which are called 'mults'.

Table 1: Some parameters related to the TEL.

Rms transverse size of electron lens	0.66 mm
Beta functions at the TEL	100 m (x), 30 m (y)
TEL current	0.6 A
TEL pulse length	1.2 $\mu$ s
TEL length	2 m

Figure 1 illustrates the timing of the proton and pbar beams at the TEL, measured when the TEL was tuned to the abort gap (therefore the TEL signal is not visible here). Only the last pbar bunch in each train has no near-synchronous proton bunch at the TEL. For this study the TEL was now timed on pbar bunches A5, A17 and A29, and the accompanying proton bunches whose index is higher by 1. Figure 2 shows the TEL currents when operated in this 3-pulse per turn mode.

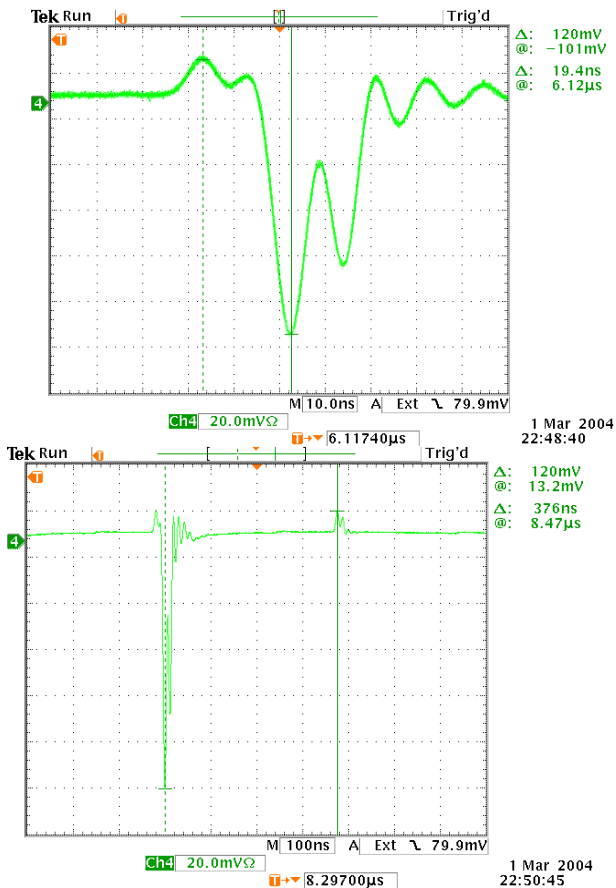


Figure 1: Top graph shows a typical proton signal at the TEL together with that of the nearest pbar bunch. The separation is about 19.4 ns. The bottom graph illustrates the distance between the last proton bunch and the last pbar bunch in the train. It is about 376ns, 20 RF buckets.

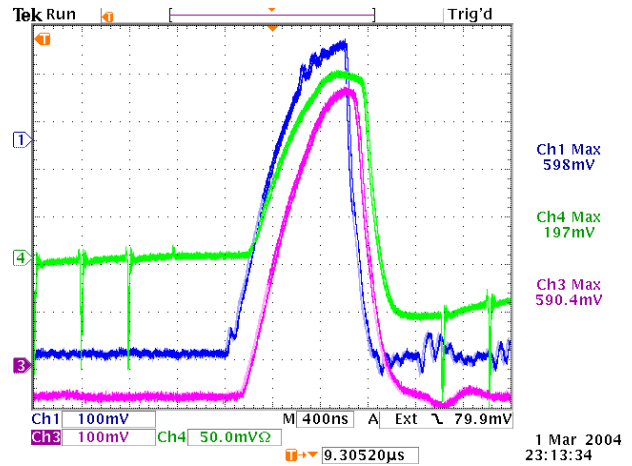


Figure 2: Signal from TEL BPM (green), TEL cathode current (yellow), and collector current (magenta), for 3-pulse per turn operation, at 23:15:21.

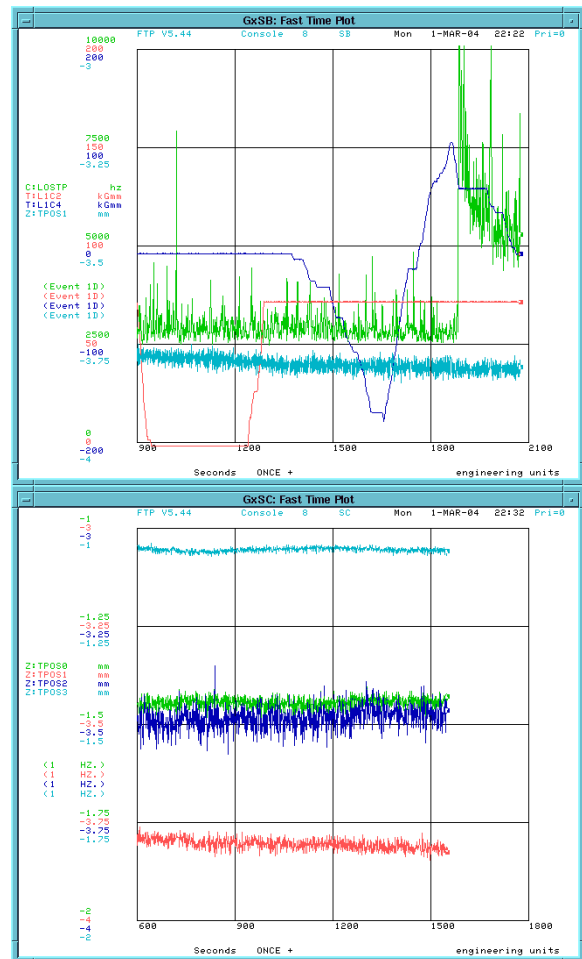


Figure 3: Proton loss rates plus TEL corrector settings L1C2 and L1C4 and 1 proton beam position reading (top picture); several beam position readings (bottom picture), during aperture scan without TEL electron beam. Changing TEL correctors by +3(4) mm did not increase proton losses. The peak at the end was due to a trip of pbar RF station 5. Beam orbit in TPOSx changed by not more than 10 microns.

To ensure that any change in loss rate etc. is due to the action of the TEL and not due to spurious orbit changes of protons or pbars, we scanned the TEL orbit correctors without TEL beam over several mm. Figure 3 shows that the loss rate was constant over the full range of the corrector scan. Residual proton orbit motion was less than 10  $\mu\text{m}$ . The steep increase in the loss rate at the end of this scan was due to the unrelated RF trip. Figure 4 displays the protons and pbar intensities and halo loss rates recorded after this trip.

Table 2: Current position readouts for the three beams at the upstream and downstream ends of the TEL.

	upstream		downstream	
	X	Y	X	Y
Protons	5.0	2.4	4.5	3.2
Pbars	0.1	1.0	-1.6	2.1
Electrons	4.0	2.6	2.6	1.5

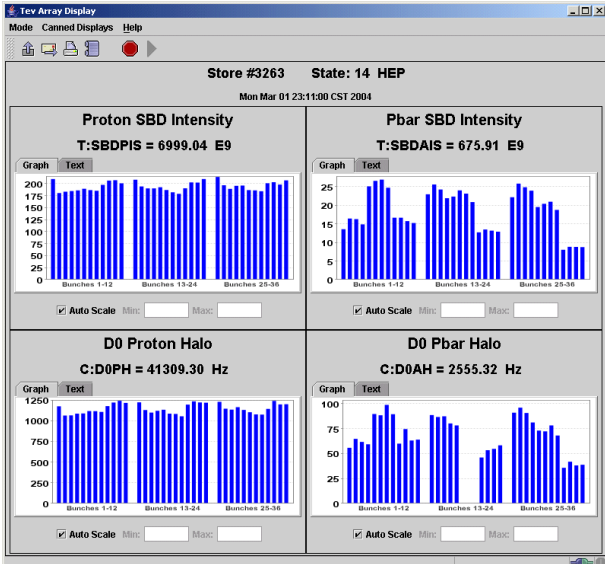


Figure 4: Proton and pbar intensities and losses after the rf trip, at 23:11:57.

### Two-Dimensional Scan

Figure 5 illustrates the TEL position scans performed during this experiment, as reconstructed from the corrector settings. The cross is the aperture scan without TEL; the two spirals represent the 2D grid scan around the pbar and proton beams.

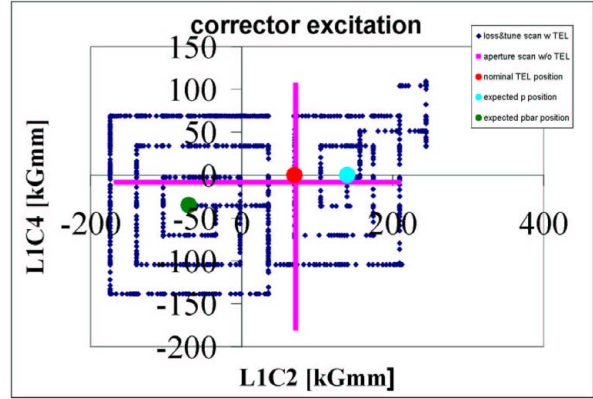


Figure 5: Corrector excitation pattern during the MD. Visible are the aperture scan without TEL in pink in the form of a cross and the 2-dimensional grid scan with TEL. Also indicated are the expected nominal positions of TEL, protons, and pbars, respectively, as (very roughly) extrapolated from the upstream TEL-BPM readings. The solenoid field is 35 kG and therefore 35 kGmm correspond to 1 mm displacement on either axis. L1C2 controls the horizontal electron position, L1C4 the vertical.

### Tune Variation

Figures 6 and 7 show the variation in pbar and proton tune, respectively, as a function of time, together with the horizontal and vertical TEL corrector settings. Figure 4 is the data of Fig. 2 plotted as a contour, and Fig. 5 is again the same data plotted as a surface. The pbar tune strongly changes with the position of the TEL. Unexpectedly, a large tune excursion is found when the TEL is close to the proton beam. The maximum tune shift of the pbars is about 0.008. The expected tune shift is estimated from

$$\Delta Q = \frac{I_e}{ev_e} \frac{r_p}{2\pi\sigma_e^2} \frac{\beta_x}{2\gamma} (1 - v_e/c) \mathcal{L}_e$$

Assuming an acceleration voltage of 6 kV, the electron velocity is  $v_e \approx 0.15c$ , and for 600 mA current and an rms transverse size of  $\sigma_e = 0.66 \text{ mm}$ , the tune shift is 0.005 for a single particle. It could be up to two times smaller for coherent oscillations of the beam centroid. It is remarkable that the pbar beam shows the largest tune shift when the TEL is near the protons. This is probably an indication of coherent proton motion, coupled via the beam-beam interaction to the pbars.

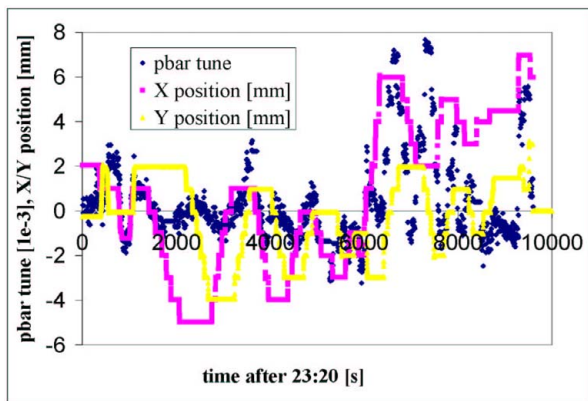


Figure 6: Variation in horizontal pbar tune from 1.7-GHz Schottky monitor in units of  $10^{-3}$  measured on the three excited bunches A5, A17 and A29 as a function of time, together with the horizontal and vertical TEL position..

Figures 8 and 9 show contour plots of the pbar and proton tunes on the two-dimensional grid. We can infer approximate positions for the two beams from these graphs. Figures 10 and 11 are more sophisticated tune contour plots for the pbars, over two different ranges. Figure 12 shows the predicted tune shift due to the TEL for a 'pencil' pbar beam. Figure 13 is a finer plot for the proton tune, after synchronizing the data. Figure 14 is yet another plot for the pbars, analyzed in a different way. Figure 15 shows a final measurement result, aimed at verifying the functionality of the tune fitter. The bare tune for both beams was varied and the tune fit exactly tracks this change for both beams.

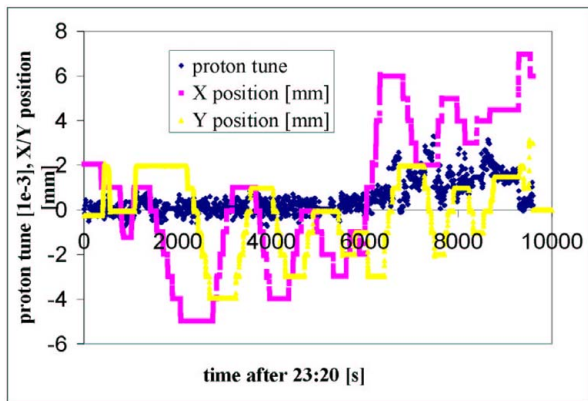


Figure 7: Variation in horizontal proton tune from 1.7-GHz Schottky monitor in units of  $10^{-3}$  measured on the three excited bunches P6, P18 and P30 as a function of time, together with the horizontal and vertical TEL position changes.

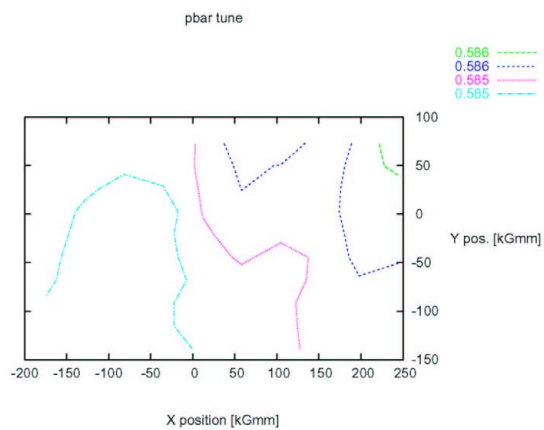


Figure 8: Contour plot of pbar tune variation as a function of transverse TEL positions, for pbar bunches A5, P17, and A29. Pbars could be at location  $-100, -50$ ?

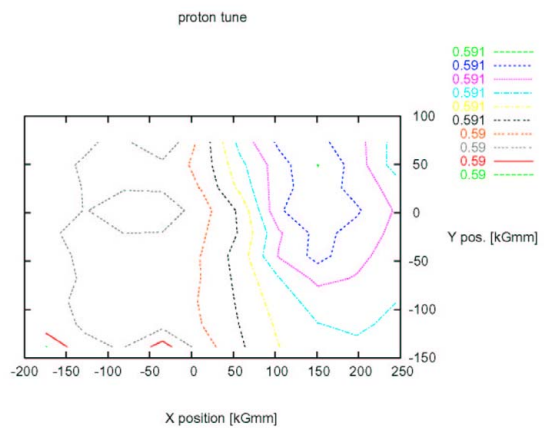


Figure 9: Contour plot of proton tune variation as a function of transverse TEL positions, for proton bunches P6, P18, and P30. Protons could be at location  $150, 50$ .

### Pbar Horizontal tune vs e-beam position

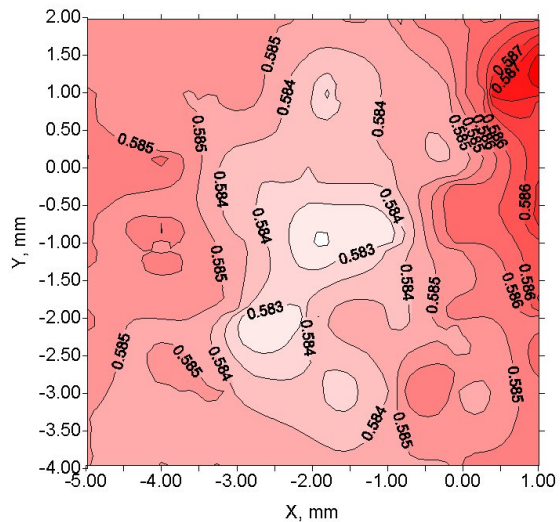


Figure 10: Pbar tune as a function of TEL position.

Pbar tune T:TULAHT vs e-beam position

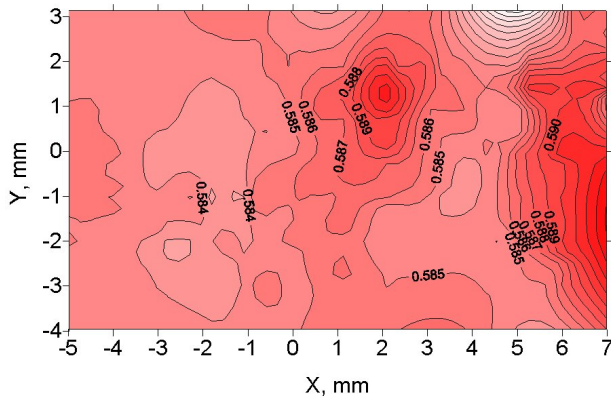


Figure 11: Pbar tune as a function of TEL position over a wider horizontal range.

Predicted tune shift due to TEL J=0.6A, sigma\_r=0.7mm

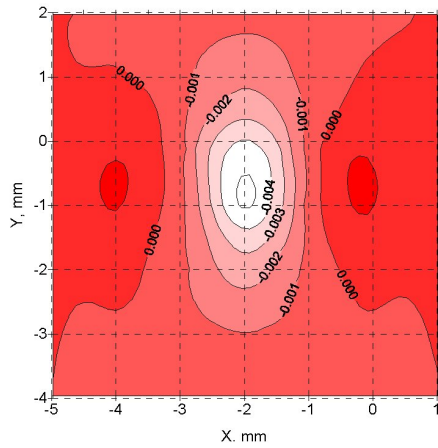


Figure 12: Predicted tune shift for pencil pbar beam.

Proton tune vs e-beam position

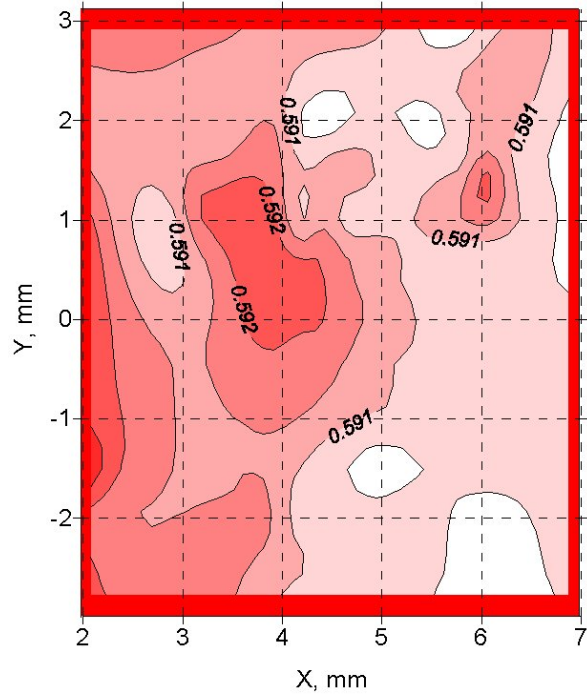


Figure 13: Proton tune as a function of TEL position.

Pbar Tune during the TEL scan.

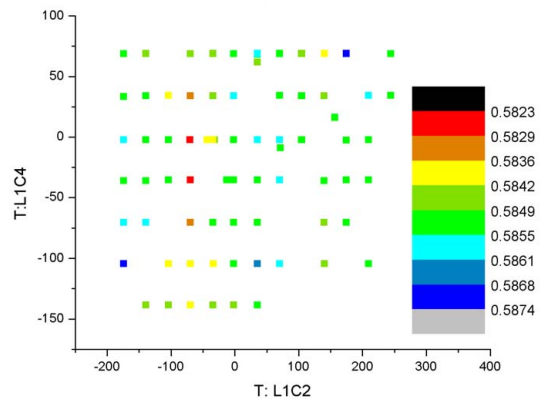


Figure 14: Pbar tune as a function of TEL corrector settings, computed by a tedious JAVA script.

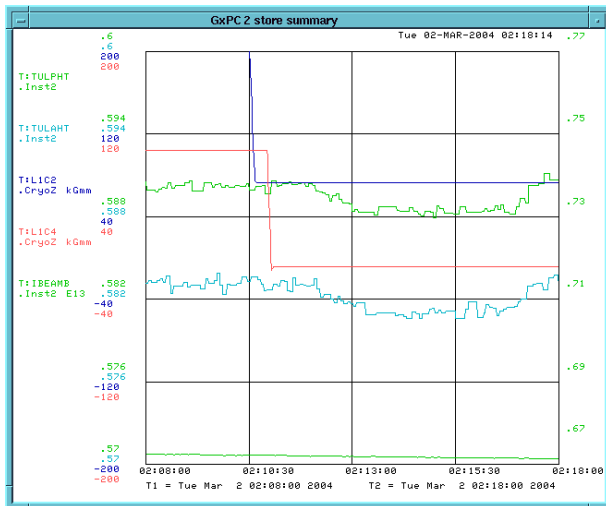


Figure 15: Response of 1.7-GHz Schottky tune fitter to a change in the horizontal base tune for protons and pbars by  $-0.002$  units.

### Schottky “Emittance”

In addition to the tune per se, the 1.7-GHz Schottky monitor also provides an ‘emittance’ number, which is proportional to the total power in the tune spectrum. Figures 16 and 17 demonstrate the variation of this emittance as a function of time. The pbar emittance strongly increases when the TEL is near the proton beam, suggesting that indeed the large tune shift was due to coherent motion driven by the protons.

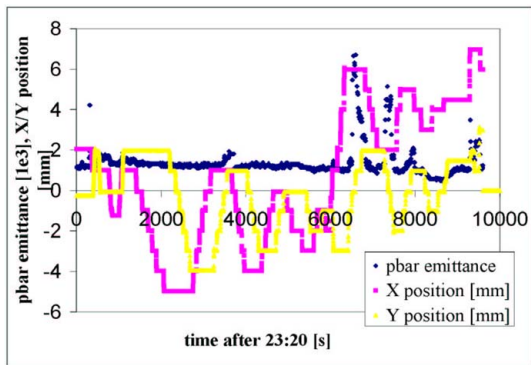


Figure 16: Variation in horizontal pbar “emittance” from 1.7-GHz Schottky monitor in (uncalibrated) units of  $10^3$  measured on the three excited bunches A5, A17 and A29 as a function of time, together with the horizontal and vertical TEL position changes.

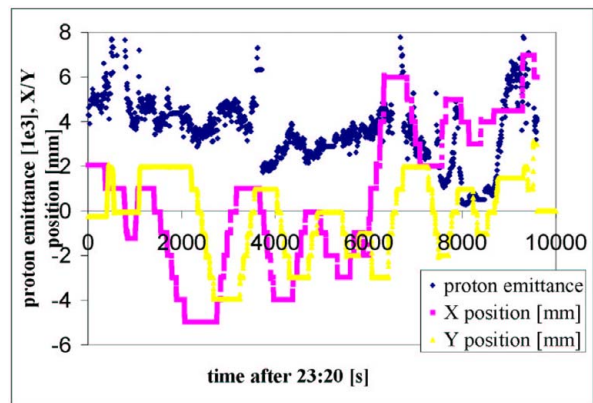


Figure 17: Variation in horizontal proton “emittance” from 1.7-GHz Schottky monitor in (uncalibrated) units of  $10^3$  measured on the three excited bunches P6, P18 and P30 as a function of time, together with the horizontal and vertical TEL position changes.

The proton emittance changed throughout the scan. We can again generate contour plots, which are shown in Figs. 18 and 19. Both emittances are clearly sensitive to TEL positions in the vicinity of the protons. The largest ‘instability’ or coherent signals seem to occur when the TEL is ‘at the edge’ of the proton beam, not when it is centered on it.

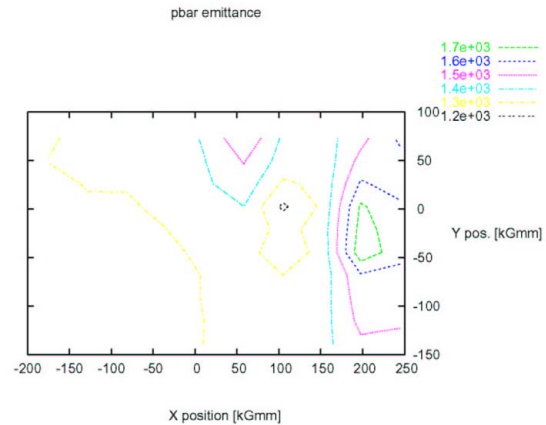


Figure 18: Contour plot of pbar emittance variation as a function of transverse TEL positions, for pbar bunches A5, A17, and A29. Pbar signal is largest when TEL is near the proton beam.

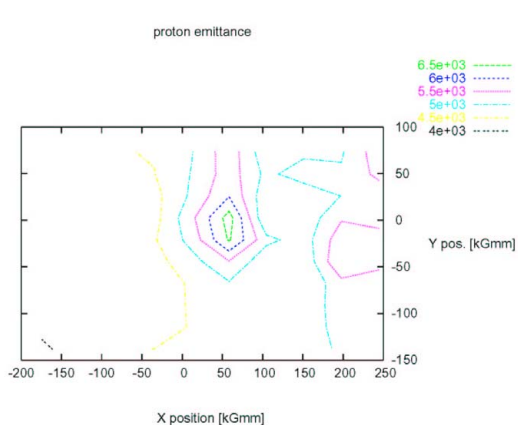


Figure 19: Contour plot of proton emittance variation as a function of transverse TEL positions, for proton bunches P6, P18, and P30.

### Losses

The proton losses depend on the setting of the TEL position as illustrated in Fig. 20. When the TEL is positioned close to the expected location of the proton beam the proton losses significantly increase. Figures 21 and 22 show contour plots of proton and pbar losses as a function of TEL position. We can easily estimate the position of pbars and protons from these plots, assuming that losses are maximum when the TEL position coincides with the beam position.

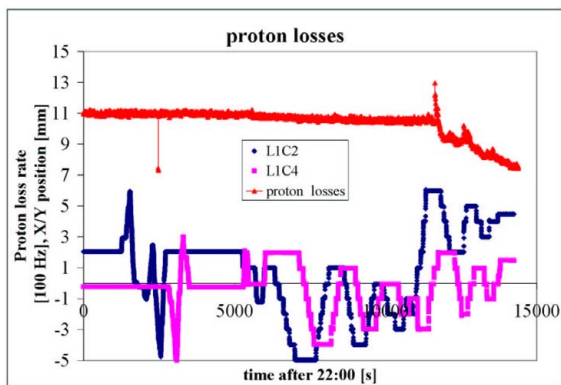


Figure 20: Average loss rate in proton bunches P6, P18 and P30 as a function of time, together with the the TEL horizontal and vertical position.

Figures 23-26 show further, more sophisticated contour plots, which even more clearly indicate the positions of the two beams. Figure 27 shows the pbar loss rate as a function of the inferred distance between TEL and pbar orbit, revealing an inverse cubic dependence. This might be the key result of our experiment.

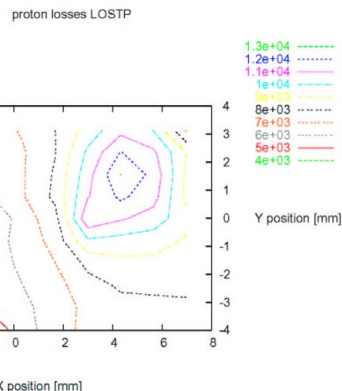


Figure 21: Contour plot of proton losses as a function of transverse TEL positions, for all proton bunches. Proton beam appears to be at location 4.5, 1.5 mm.

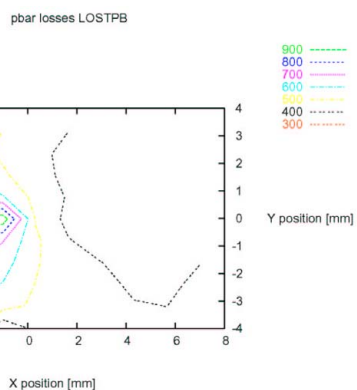


Figure 22: Contour plot of pbar losses as a function of transverse TEL positions, for all pbar bunches. Pbar beam appears to be at  $-2$  mm, 0 mm.

### Pbar losses C:D0AHTL vs e-beam position

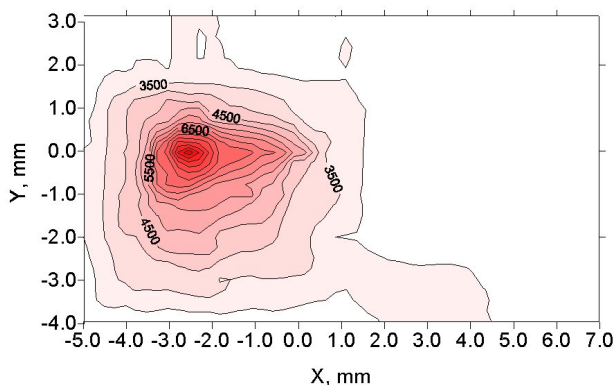


Figure 23: Contour plot of all pbar losses vs. TEL position.

D0AH[5] while TEL was in vicinity of pbars

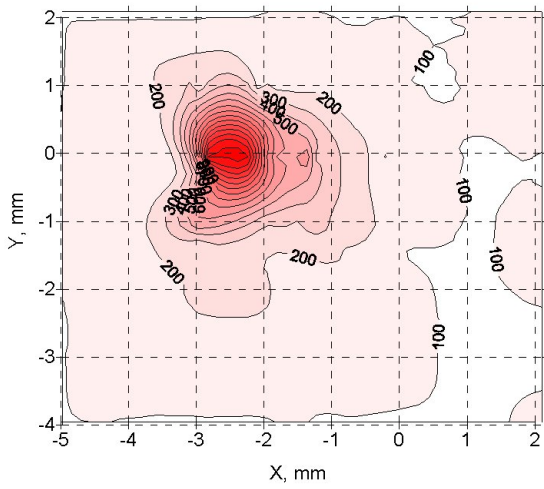


Figure 24: Contour plot of individual pbar A5-bunch losses vs. TEL position.

Proton Losses C:LOSTP vs E-beam Position

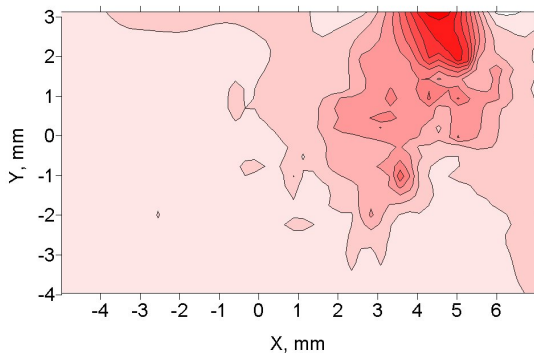


Figure 25: Contour plot of proton losses vs. TEL position.

Proton losses vs e-beam position

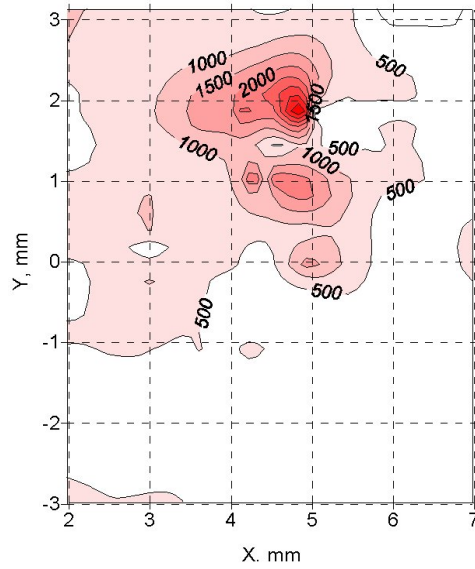


Figure 26: Contour plot of proton losses vs. TEL position after better synchronization.

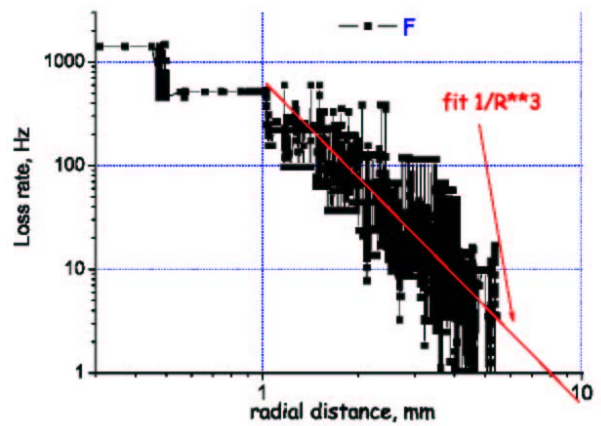


Figure 27: Antiproton loss rate as a function of TEL distance, exhibiting an inverse cubic dependence.

## Bunch Length

The proton bunches were shaved longitudinally, when the TEL approached. The shaving of bunches 4, 5 and 6 was evident on the Tevatron SBD display; see Fig. 28. Figures 29-31 show the time evolution of the bunch lengths during the MD and the dependence on TEL position as contour plots (the proton bunch length has a contour since the beam was shaved progressively while approaching the proton beam). The bunch lengths in these figures are average over all bunches. The shaving effect is more visible, if the length of individual bunches is considered. These are shown in Figs. 33 and 34 for protons and antiprotons, respectively. In each picture one bunch interacts with the TEL, while the other does not.

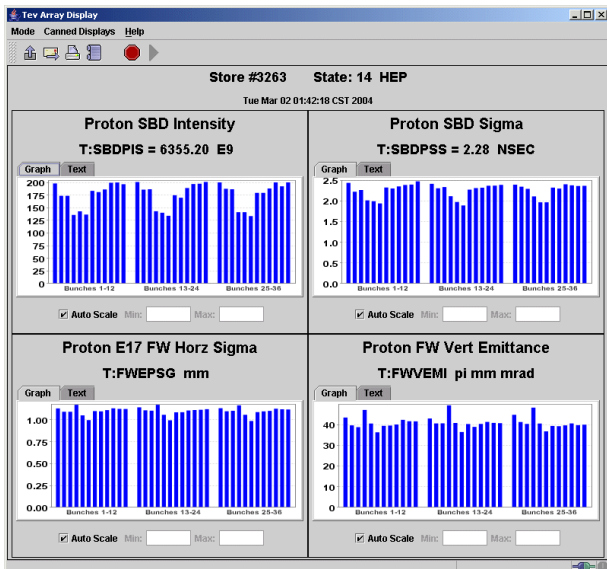


Figure 28: Proton intensity, bunch length and transverse sizes for all proton bunches. The bunches affected by the TEL, e. g., P4, P5, and P6 (the TEL pulse is too long to excite a single bunch, but in total spans about 3 bunches, with maximum amplitude at P6), show a decrease in intensity and a decrease in bunch length.

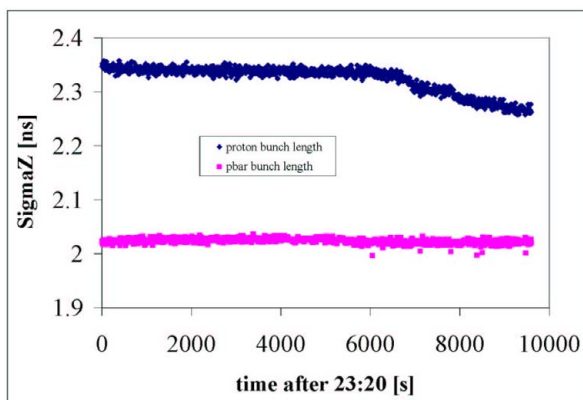


Figure 29: Bunch length from BDS Gaussian fit as a function of time, averaged over all proton and pbar bunches. The proton beam is shaved longitudinally

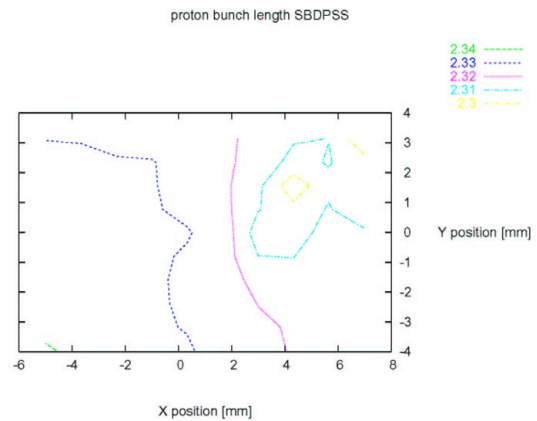


Figure 30: Contour plot of proton bunch length as a function of transverse TEL positions, for all proton bunches.

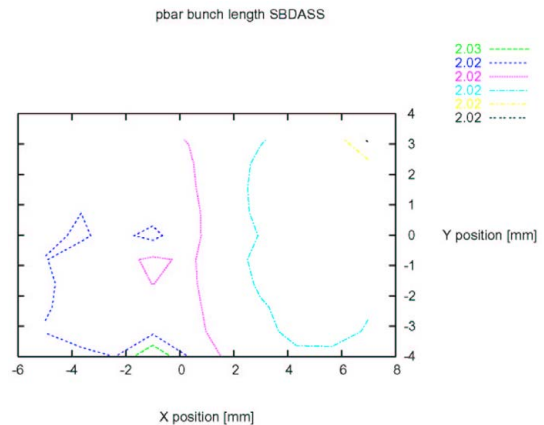


Figure 31: Contour plot of pbar bunch length as a function of transverse TEL positions, for all pbar bunches.

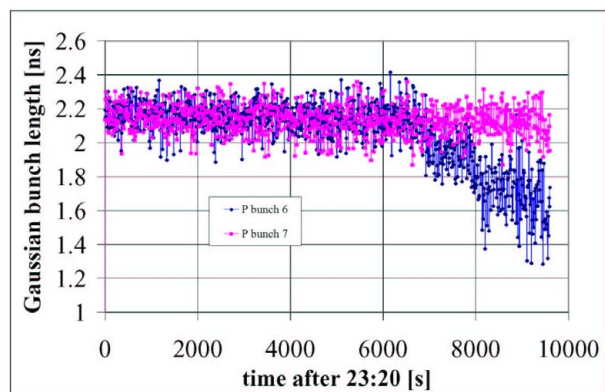


Figure 32: Bunch length from BDS Gaussian fit as a function of time for proton bunches P6 and P7. The bunch P6 which interacts with the TEL is shaved longitudinally.

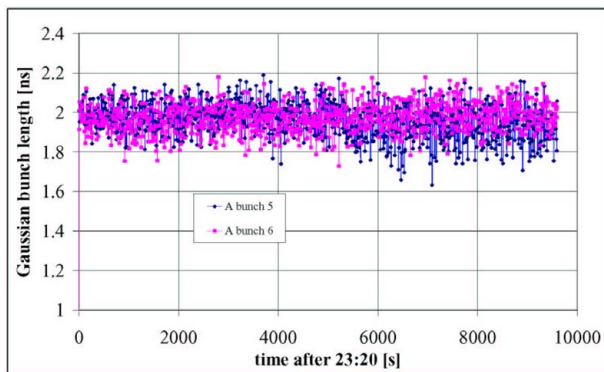


Figure 33: Bunch length from BDS Gaussian fit as a function of time for pbar bunches A5 and A6. The length of bunch A5 which interacts with the TEL does not change noticeably.

### Wire Scans

Figure 34 shows the flying wire scan for pbar bunch 5 before the start of the TEL scan. The size is 0.712 mm vertically and 0.797 mm horizontally. Figure 35 is the same plot, measured after the pbar scan. The pbar sizes now are 0.733 mm and 0.801 mm, respectively. Figure 36 finally shows the pbar size after the proton scan. They are now 0.746 mm and 0.794 mm. It appears as if there was some blow up in the vertical plane. The sizes for proton bunch 5 are very slightly reduced (note, however, that proton bunch 6 was the one that was mostly excited).

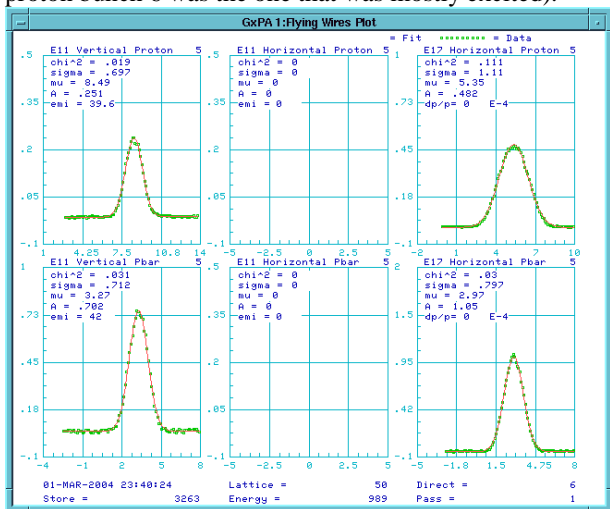


Figure 34: Flying wire scan for pbar bunch 5 before starting the TEL scan, 23:41:42.

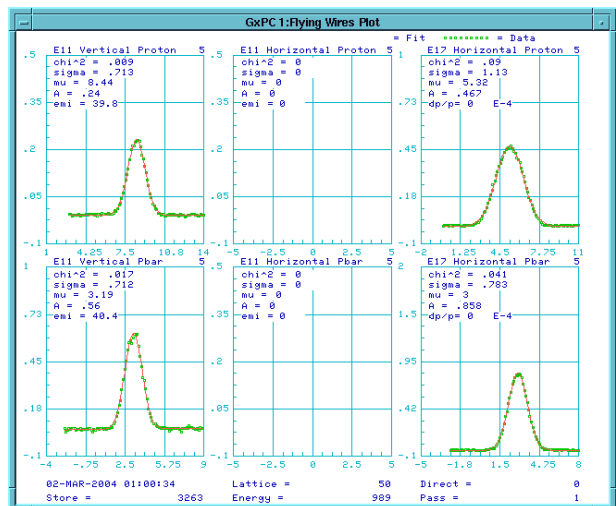


Figure 35: Flying wire scan for pbar bunch 5 before starting after TEL scan on pbars, 01:03:01.

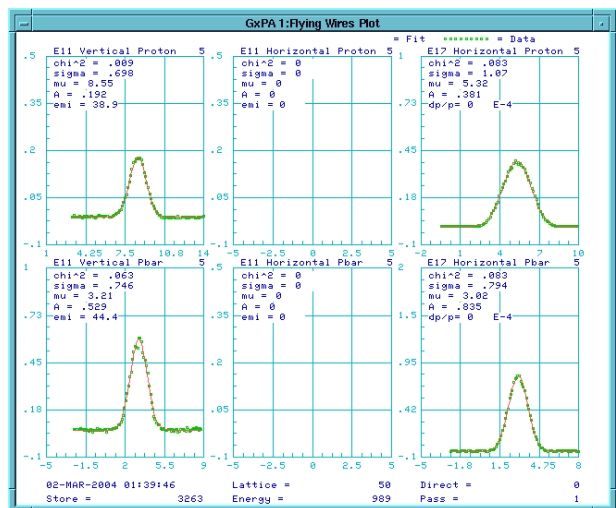


Figure 36: Flying wire scan for pbar bunch 5 before starting after TEL scan on pbars, 01:46:01.

## SL Emittances

Figures 37 to 40 show contour plots for the four transverse emittances from the synchrotron-light monitor.

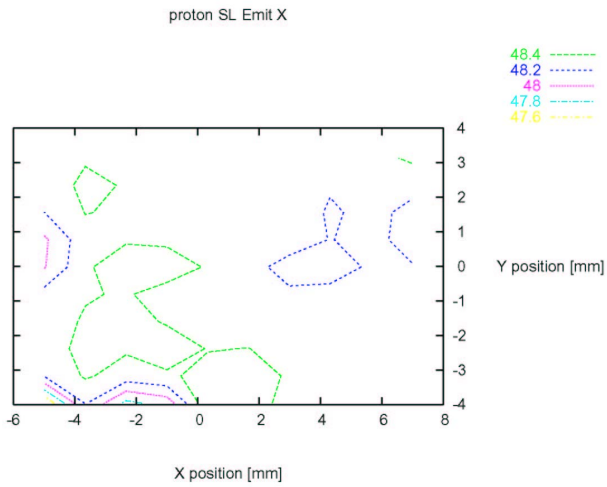


Figure 37: Contour plot of horizontal proton emittance from SL monitor as a function of transverse TEL positions, for all proton bunches.

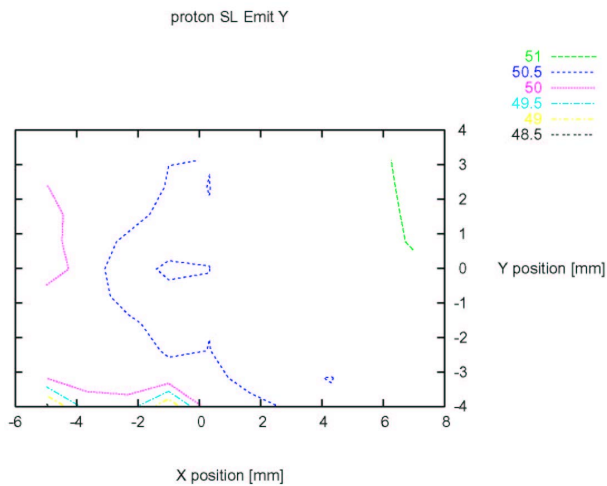


Figure 38: Contour plot of vertical proton emittance from SL monitor as a function of transverse TEL positions, for all proton bunches.

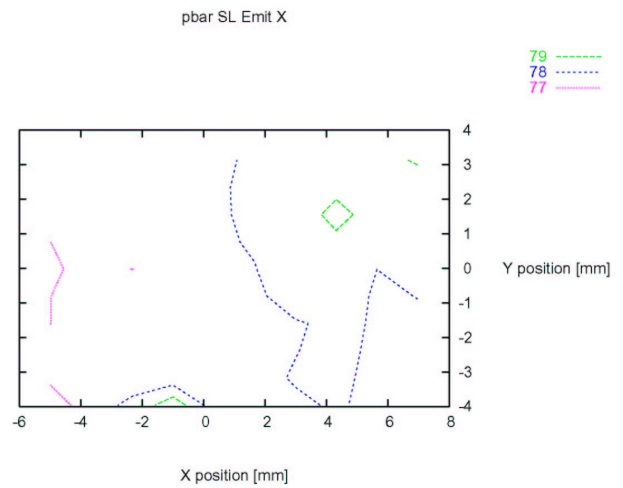


Figure 39: Contour plot of horizontal pbar emittance from SL monitor as a function of transverse TEL positions, for all pbar bunches.

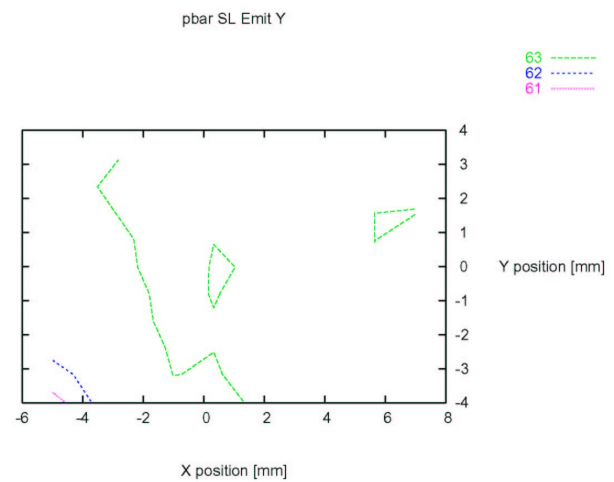


Figure 40: Contour plot of vertical pbar emittance from SL monitor as a function of transverse TEL positions, for all pbar bunches.

### Old Schottky Signal

Figures 41-46 show horizontal and vertical Schottky spectra from the old monitor taken at various times during the scan across pbars and protons. Clearly visible are a large number of synchrotron sidebands in both planes. The spectra strongly change with the TEL position; compare, e.g., the vertical spectra in Figs. 43 and 44.

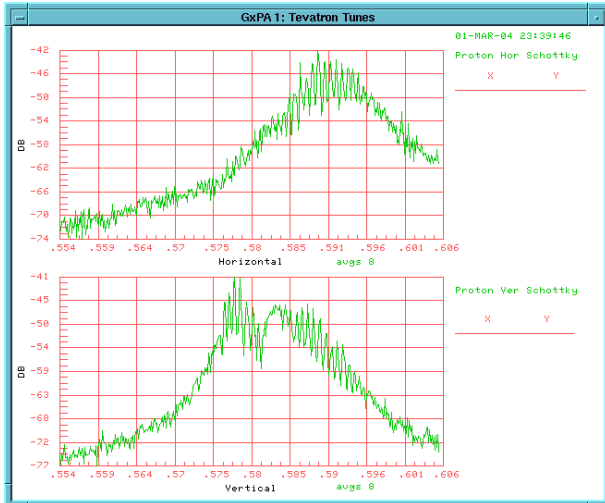


Figure 41: Horizontal and vertical spectrum from old Schottky monitor, with TEL at -1 mm, +2 mm from starting point.

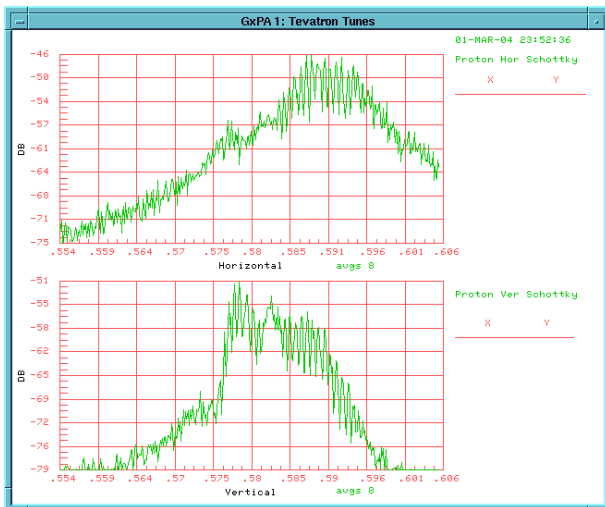


Figure 42: Horizontal and vertical spectrum from old Schottky monitor, with TEL at -6 mm, +2 mm from starting point.

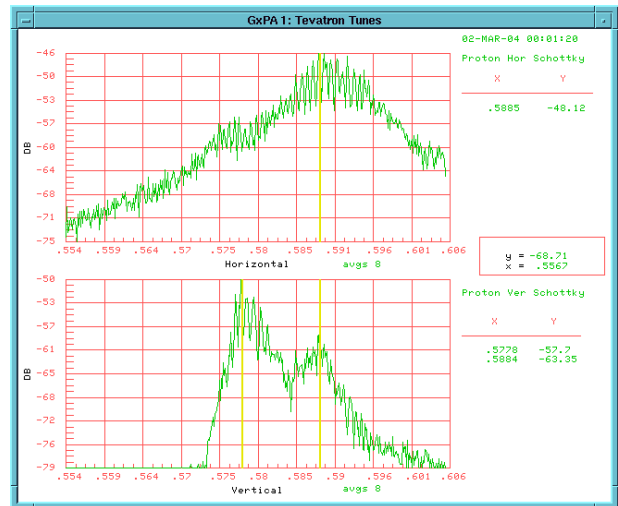


Figure 43: Horizontal and vertical spectrum from old Schottky monitor, with TEL at -7 mm, -1 mm from starting point.

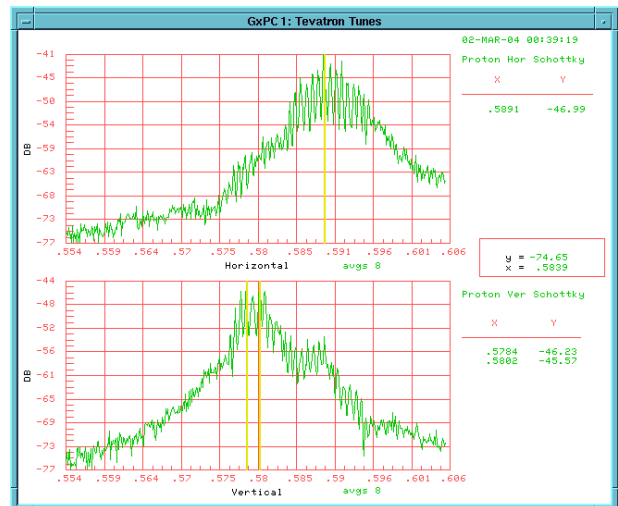


Figure 44: Horizontal and vertical spectrum from old Schottky monitor, with TEL at -2 mm, -2 mm from starting point.

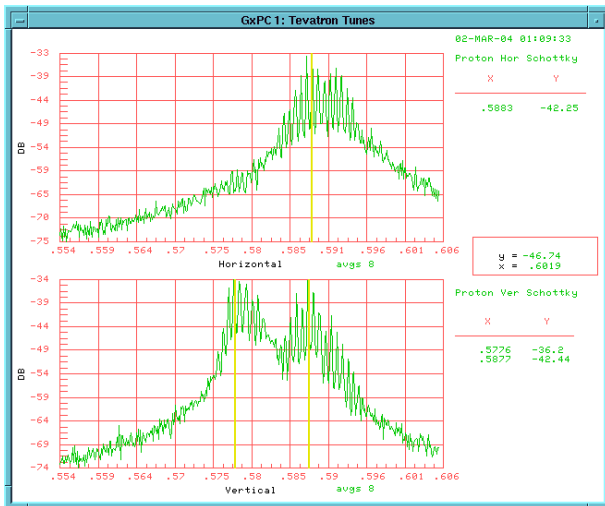


Figure 45: Horizontal and vertical spectrum from old Schottky monitor, with TEL at +4 mm, 0 mm from starting point.

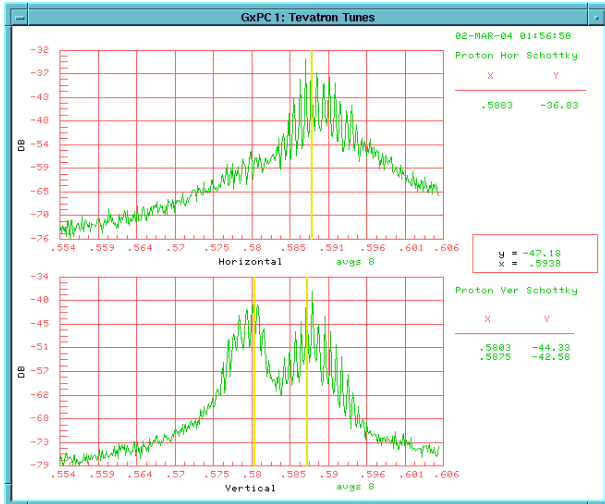


Figure 46: Horizontal and vertical spectrum from old Schottky monitor, with TEL at +5 mm, +2 mm from starting point.

### Proton and Pbar Position Relative to the TEL

Figure 47 summarizes the TEL scan performed in this experiment. Beam sizes are also indicated. Beam positions are shown as inferred from the sophisticated contour plots. Positions of the TEL with respect to protons and pbars as determined from TEL BPMs are compared with those inferred from the more primitive contour plots for tunes and losses in Table 2. Table 3 lists the implied distances between protons and pbars.

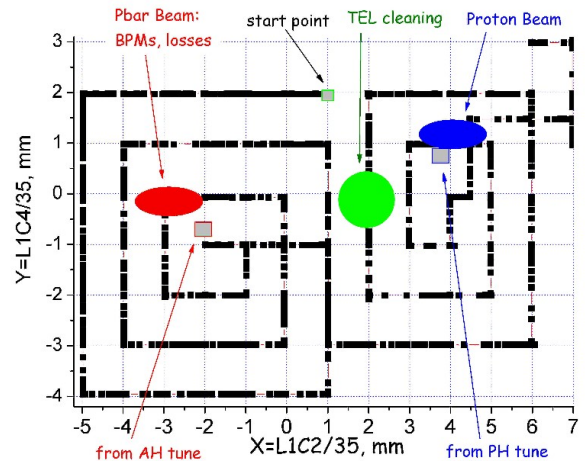


Figure 47: Summary of TEL position scan. Beam sizes are approximately to scale.

Table 2: Relative transverse position of proton and pbar beam with respect to the nominal TEL location, as inferred from upstream (U) and downstream (D) BPMs, from the tune variation on the two-dimensional grid scan, and from the loss-rate variation for the same scan.

	X	Y
TEL BPM (U+D)	3.3 mm	2.05 mm
P BPM (U+D)	4.75 mm	2.8 mm
Pbar BPM (U+D)	-0.75 mm	1.55 mm
$\Delta$ (P-TEL) BPM	1.45 mm	0.75 mm
$\Delta$ (Pbar-TEL) BPM	-4.05 mm	-0.55 mm
$\Delta$ (P-TEL) tune	2.26 mm	1.69 mm
$\Delta$ (Pbar-TEL) tune	-4.89 mm	-1.2 mm
$\Delta$ (P-TEL) LOSTP	2.37 mm	1.76 mm
$\Delta$ (Pbar-TEL) LOSTPB	-4.03 mm	0.26 mm

Table 3: Transverse distances between proton and pbar beams, as inferred from Table 2.

	X	Y
$\Delta$ (P-Pbar) BPM	5.50 mm	1.30 mm
$\Delta$ (P-Pbar) tune	7.15 mm	2.79 mm
$\Delta$ (P-Pbar) loss rate	6.40 mm	2.02 mm

## **PRELIMINARY CONCLUSIONS**

The measured tune shifts of protons and pbar are compatible with expectation.

The proton Schottky 'emittance' is strongly dependent on the TEL position, possibly due to a coherent interaction between protons and electrons.

The positions of protons, pbars and TEL were determined in three different ways: from the TEL BPM readings, from the tune variation with TEL position, and from the loss-rate variation with TEL position. The various results are consistent at least within 1 or 2 mm, possibly better. Tunes and losses do not necessarily give exactly the same value for the beam position.

Significant proton losses occurred when the TEL approached the proton beam. These losses decreased with the third power of the distance. They were the result of a longitudinal shaving, which might be related to a longitudinal interaction of TEL and proton beam and/or to the nonzero dispersion at the TEL.